Autonomous Burrowing and Retrieval of Soft Robotic Anchors in Granular Media

Dongting Li[1], Michael T. Tolley[1,2] and Nick Gravish[*,1,2]

Abstract— **Vertical digging into and out of granular media is a challenging task for autonomous systems. Granular media present considerable resistance to vertical penetration due to the high friction forces and large pressure at depths. In this paper, we present a soft robot that is capable of digging into and out of granular media to depths over 10× its body length. Our robot incorporates a vibration motor to locally fluidize the granular media for burrowing, and a soft pneumatic actuator to adjust the volume and hence the density of the robot, allowing it to transition from digging down to digging up. To analyze the performance of the robot, we measure its weight and density, track its location using a motion capture system, and investigate the effect of local fluidization. When the robot is buried and inflated with vibration turned off, it can increase its passive anchoring force by 5.22× (up to 35 N) relative to when the robot is deflated with vibration on. By contrast, by inflating the soft pneumatic bladder and providing vibration the robot is able to actively unburrow.**

Keywords: Soft Robot Design, Soft Robotics Application, Granular Media Locomotion, Digging Robot

I. INTRODUCTION

Digging in resistive media such as granular materials and mud has presented a significant challenge to the field of robotics in recent decades. Achieving depths of even 10 cm proves difficult for most robots [1], [2]. Considering the ratio of digging depth to body height, some state-of-the-art robotic or digging devices are capable of digging up to 1000 mm or a ratio of depth to body height of up to 3× [3].

The Scallop Theorem, which states that reciprocal movement in resistive media like sand does not produce net displacement [4], has prompted researchers to develop robots that break this symmetry for effective locomotion [5], which can be done by adjusting the robot's shape during a burrowing cycle. For example, Li et al [6] developed an origami-inspired fin with single-sided joint limit using one-shot 3D printing. In a full sweeping cycle, asymmetric deformation occurs generating forward motion. Similarly, Chopra et al [7] utilized joint limits on flexible appendages to bias the drag force on the arm towards forward locomotion. Although a majority of these robots focus on horizontal locomotion, such as swimming and crawling, the underlying principles can be applied to vertical motion. Besides these passive, pre-programmed shape deformations, Tao et al [8] introduced a razor calm inspired self-unburrowing robot that can actively tune its shape during digging/unburrowing cycle. Asymmetric geometry for digging, such as screw or auger inspired digging devices have also been demonstrated [9], [10].

Local fluidization of granular material [11] offers another approach to burrowing by reducing drag and resistance within the surrounding media. Researchers have developed various robots employing this principle for vertical digging, forward everting, and other locomotion strategies [12]. A common method for achieving local fluidization involves ejecting fluid (water or air) into the granular media (GM). Naclerio et al [13], [14] integrated air ejection device at the tip of an underground growing vine robot which significantly reduces the drag in underground locomotion. Similarly, water jetting in granular media can also reduce the resistance for vertical intrusion [15].

Another less explored approach in robotics research involves using vibration for local fluidization [16], [17]. While vibration has shown promise for surface granular media tank fluidization [18], surface locomotion [19], and reducing penetration resistance [20], its application in minimizing drag and friction for robotics digging/unburrowing remains relatively unexplored.

Recent research has demonstrated that Archimedes' principle can be extended to describe the penetration of solid objects into granular media [21]. Archimedes' principle states that an object submerged in a fluid experiences an upward buoyant force equal to the weight of the fluid displaced. A related phenomenon, known as granular convection or the Brazil nut effect, describes how larger particles within a vibrated or shaken granular bed tend to rise to the surface. This upward movement is a result of fluidization, where the granular material behaves like a fluid. However, Shinbrot suggested that, with a larger intruder in globally air-fluidized granular media, a "Reverse Brazil Nut Effect" occurs, meaning that the object sink to the bottom instead of floating under ideal condition [22]. While robot vibration has been used to generate locomotion on the surface of granular material [19], to the best of our knowledge, a physical robotic prototype utilizing this principle for vertical locomotion in granular media has not yet been developed. These concepts lead to a promising avenue: by fluidizing granular media and controlling the density and/or shape of a robotic device as illustrated in Fig. 1(a), can we achieve digging with modulate between high and low density profiles for burrowing and unburrowing with the same robot?

To develop a self-propelling robot capable of burrowing and unburrowing using vibratory fluidization, we sought to use local vibration and volume change as complementary

[1]Department of Mechanical and Aerospace Engineering at the University of California, San Diego (UCSD), 9500 Gilman Dr, La Jolla, CA, 92093, USA, [2] Materials Science and Engineering Program, University of California San Diego, La Jolla, CA, 92093, USA; * Corresponding Author; dongtingli@ucsd.edu, tolley@ucsd.edu, ngravish@ucsd.edu.

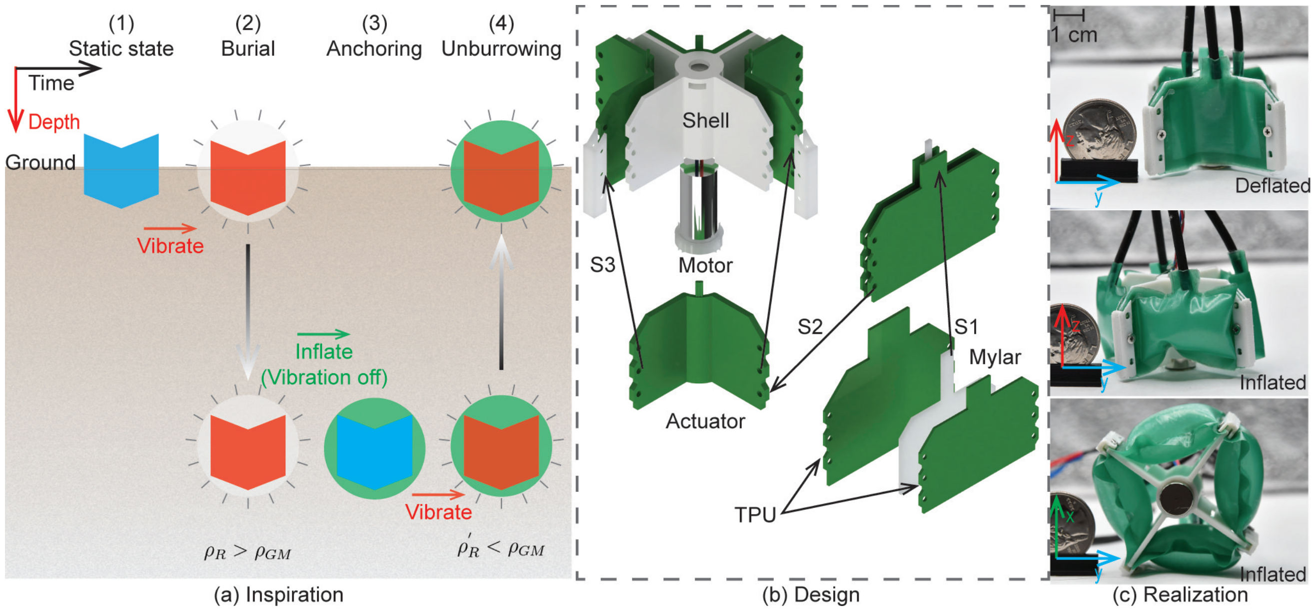

Fig. 1: (a) illustrates concept for burrowing, anchoring and unburrowing leveraging vibration-based fluidization and volume change. We indicate the vibration by color, where blue means the vibration is off and red stands for vibration engaged. (a2): During the burial process, the robot vibrates, which fluidizes the surrounding sand and allows the robot to sink into the sand. (a3): The robot then anchors (increases the force required to remove it from the sand) by inflating its body and displacing the sand locally (indicated by the transparent green circle and black lines). (a4): Finally, the inflated robot unburrows by locally fluidizing the sand with vibration, since the average density of the robot at this point is less than that of sand, the robot "floats" to the surface when the sand is fluidized. (b) details the robot's design, including manufacturing and assembly processes. (c) compares the robot prototype in deflated and inflated states, with height relative to a 25.4 mm diameter quarter dollar coin (1 inch).

control inputs. Controlling the density or volume of a body, whether a biological organism or a robotic vessel, in fluids like water can be achieved through mechanisms such as internal bladders such as swim bladder in fishes or by adjusting the overall body volume. This robot utilizes vibration for local fluidization to achieve both digging and unburrowing in granular media.

Inspired by these principles, we introduce a robotic prototype with adjustable volume/density using a soft pneumatic pouch actuator. This prototype utilizes vibration-induced local fluidization to enable downward digging, effectively reducing drag forces within the granular media. The robot is equipped with soft pneumatic actuators for volume adjustment, facilitating unburrowing. The remainder of this paper is organized as follows: Sec. II formalizes the design inspiration, introduces the robot design, and details its physical implementation. We also present the experimental setup for measuring various parameters of the prototype robot, including: volume/density, and locomotion distance/speed. In Sec. III, we conduct locomotion experiments to measure the distance traversed during digging and unburrowing cycles, demonstrating that volume tuning must be combined with local fluidization for effective unburrowing. Finally, Sec. IV concludes the paper and outlines future work.

II. Materials and Methods

A. Locomotion strategy inspiration

Our locomotion strategy is formulated around the assumption that the robot will remain stationary within granular media (GM) until it is locally fluidized by either vibration or body expansion, which can enable either digging or unburrowing respectively as illustrated in Fig. 1(a). With vibration, the robot locally fluidizes the granular media, creating a low-density zone where $\rho_R > \rho_{GM}$, allowing sinking. Inflating the robot, indicated by the green circle around the robot, increases its volume and decreases its density so that $\rho_R' < \rho_{GM}$. With fluidization, the robot in this low-density state unburrows due to buoyancy.

B. Robot design

We designed a simple, minimally viable prototype robot capable of fluidization and changing its volume. A vibration motor [1] served as the vibration source and was attached to a custom 3D-printed case. Four fins, as shown in Fig. 1(b) equally spaced around the robot body, were incorporated to prevent spinning by providing anchoring points within the granular media and extend the vibration's influence to a larger volume, facilitating local fluidization . The motor wires were routed through the center of the case to an external power supply.

To enable density tuning, pneumatic pouch bladders with side air inlets were mounted to the fins using fasteners. Each bladder was fabricated by heat-sealing two Thermoplastic polyurethane (TPU) films with a non-sticky Mylar layer sandwiched between them, creating seams along the sides, as illustrated in Fig. 1(b). Fig. 1(c) compares the assembled robot prototype in its deflated and inflated states to a 25.4

[1] Model NFP-E1015, MicroDCmotors, (diameter 11 mm, height 26 mm)

mm (1 inch) coin and table I provides the final dimensions of the robot design.

Parameter	Value	Unit
Height	30	mm
Width	30	mm
Weight	26.8	g
Power	3	W
Pneumatic actuator number	2-4	
Deflated state density	1.576	g/cm_3
Granular media density	1.568	g/cm_3

TABLE I: Robot dimension and parameter

C. Density measurement

We selected glass beads[2] (average diameter: 0.25 mm) as the granular media in our current setup, with a measured density of 1.568 g/cm^3 and prepared in a loosely packed state [23]. We then measured the density of the robot by placing the robot in water and measuring the change in water level, we obtained an average density of 1.576 g/cm^3 for the deflated robot (based on 3 measurements). With any inflation for the soft pouch actuator, the robot density will decreased under the sand density. We did not measure the density of the inflated robot since the expansion pressure can lead to complex deformations and the actual volume of the deployed pouch is not controlled.

D. Robot control and digging height measurement experimental setup

The vibration motor in the robot was controlled using a DC power supply, while the tubing from the bladders is connected and routed to a digital pressure regulator. During the burrowing process, the robot is positioned vertically in the center of the media container, and then digging is initiated.

Fig. 2 presents the granular media container used in our experiments. To ensure repeatability, we employed an air fluidization bed to prepare the dry sand. Before each experiment, an air blower fluidized the sand through a porous plate at the bottom of the container, initializing the sand to a consistent packing ratio. In these experiments, the total height of the sand was 300 mm. A custom T-slot system mounted to the bed facilitated the attachment of pulleys, through which a tendon (soft fishing line) was routed. The robot was attached to one end of the pulley, while a reflective marker was attached to the other end, as shown in Fig. 2(a). Another marker was installed at the centroid of the right pulley. By calculating the distance between the two markers, we determined the distance traveled by the robot.

We utilized a motion capture (MoCap) system[3] to track height changes. The MoCap cameras were mounted on the ceiling of our lab space and are therefore not shown in Fig. 2.

[2]BALLOTINI Blast Media: Glass Beads, 50 to 70 Mesh
[3]NaturalPoint OptiTrack with 4x Prime 13 w cameras

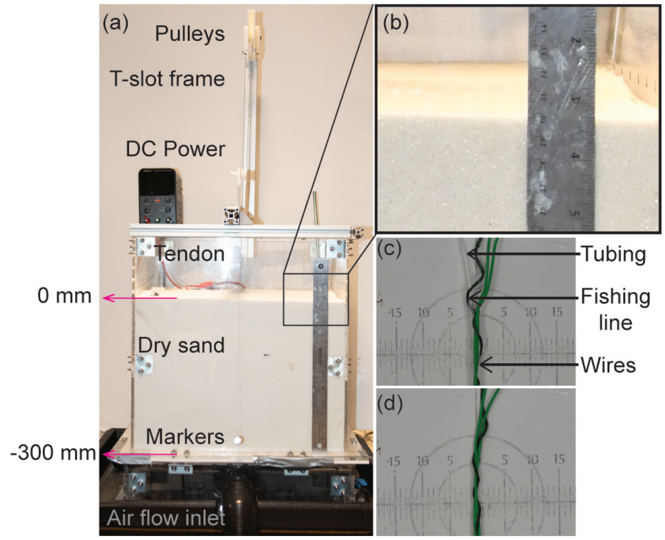

Fig. 2: Digging height/depth measurement experimental setup. (a) presents the test setup with (b) highlights the depth of the sand. In (c) and (d), we show the tether for unburrowing and digging experiments. Raw cables (wires, fishing line and tubing) are braided together, where tubing is only applied in unburrowing experiments.

III. Digging/Unburrowing experiments

A. Dry sand digging experiments

For digging into the sand, we anticipated that a streamlined, dense shape would be the most effective. However, to later increase the density of the robot, we required additional volume tuning components such as the TPU pouch actuator. To analyze the impact of this add-on mechanism on digging performance, we first measured the sinking/digging speed of the robot in two configurations: 1) with the vibration shell, pouches, and tubing, and 2) with the vibration shell only. Using the setup described in Fig. 2(a), we recorded the height change of the tracking marker as a measure of digging distance. The results, presented in Fig. 3, where 0 mm corresponds to the ground plane and negative depths correspond to downward digging. With the vibration shell only the robot was able to dig to the bottom (-300 mm) in an average of 160 s, equivalent to 0.0625 body length per second (Fig. 3, blue dot dashed line).

The addition of TPU pouches to the robot significantly impacted its digging performance. With TPU pouches attached to the robot, shown as the solid green line, the digging speed and height was significantly reduced, requiring 1440 seconds to travel up to 260 mm at an average digging speed of 0.0056 body-heights-per-second. During the experiments, we placed the robot so that its top was aligned with the ground plane. As a result, the total digging distance was the height of the robot plus the total distance traveled. We thus calculated the digging depth to be 290 mm and speed of 0.0067 body-heights-per-second.

We attribute the reduction in the digging speed of the robot with TPU pouches to the high friction generated between the TPU material and the small-diameter granular media. The soft, elastic pouch in the deflated state could have also behaved like a damper, reducing the vibration power transmitted from the motor to the granular media. To expedite the experimental process and allow for focused investigation of digging and unburrowing behaviors independently, we investigated digging and unburrowing separately, as detailed in the following sections.

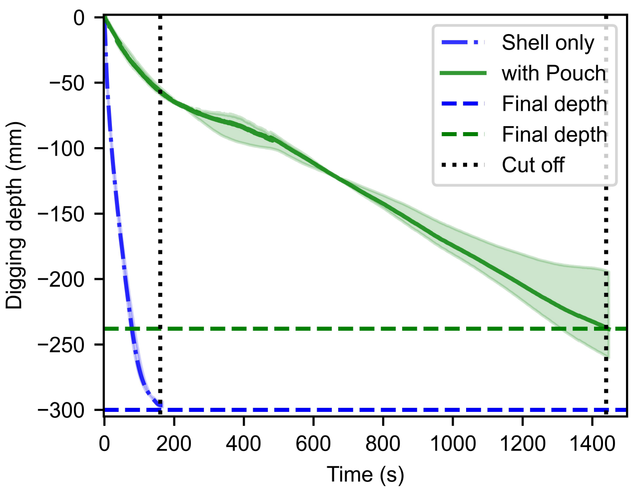

Fig. 3: Results of experiments measuring the digging rates of the robot with and without bladder actuator. In this figure, 0 mm corresponds to the ground plane (i.e., the surface of the sand). The solid lines represent the average depth versus time, while the shaded regions represents the 1 STD error bar. We compare the digging height with and without volume control components. The dashed horizontal lines represent the final depth of the two experiments, while the black vertical dotted lines indicate where the robot stop digging.

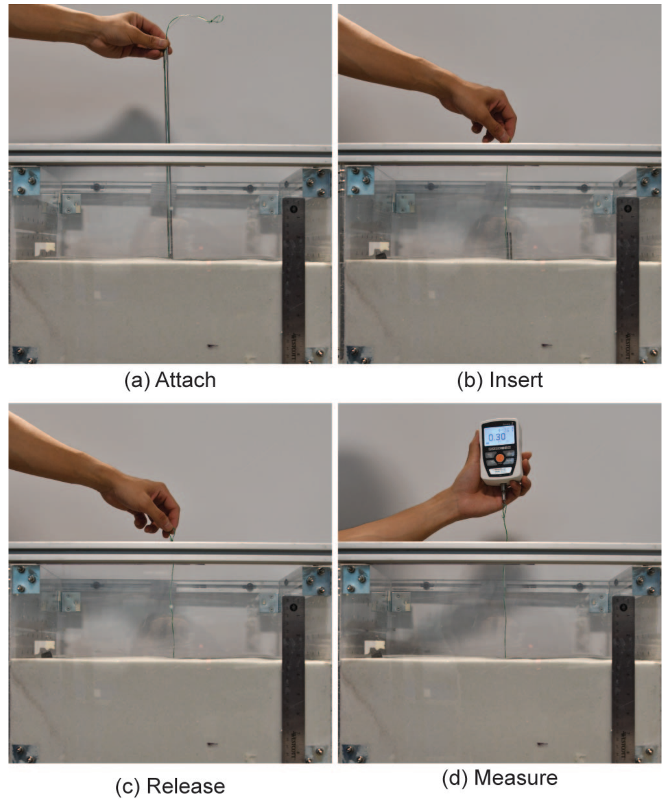

Fig. 4: Tendon friction measurement. We first attached the tendon with cable in (a) then inserted the rod to the sand while fluidizing in step (b). After inserting, we removed the metal rod as shown in (c) then pulled the tendon to record the max friction.

B. Dry sand unburrowing experiments

To characterize the unburrowing performance we first measured the tether-induced friction to determine the appropriate counterweight for these experiments. The robot is tethered to several sources during burial (i.e., wires, tubing, and tendons for power and actuation, seen in Fig. 2(c)) and we wanted to consider how these may affect the unburrowing capabilities.

Initially, we fluidized the granular media by blowing air through the bottom of the sand box. During fluidization, the resistance and friction from the granular media was minimized. We then attached the tether to a metal rod, ensuring the tendon remained straight, and stopped the fluidization. This allowed the granular media to solidify and settle, creating a frictional environment similar to that experienced during unburrowing. The metal rod was then removed, and a pulling test was conducted using a force gauge to record the maximum tension, representing the tether-induced resistance.

The average maximum force measured at 300 mm depth that the tethers resist during unburrowing was measured as 0.72 N. To compensate for the additional resistance encountered during unburrowing, we added a 70 g weight to the tip of the tendon. This counterweight sought to counteract the resisting force due to the friction and resistance between the tether and granular media and better approximate unburrowing performance the robot would experience in a real-world untethered scenario. It is worth noting that the measured resistance decreased as the tendon was pulled out of the sand, as less of the tendon was in contact with the sand, reducing friction. However, we opted to use the maximum measured force for counterweight. As the pressure, stress, and granular friction decreased as the robot approached the surface, providing this initial compensation confirmed the robot's ability to unburrow at this depth. The counterweight is only added for the unburrowing experiments which required tubing for pouch inflation, unlike the digging experiments.

During the unburrowing experiments, we manually positioned the robot at the bottom of the container while fluidizing the granular media. Similar to the counterweight selection experiments, we stopped the airflow once the robot reached the bottom to fix its position. This ensured consistent experimental conditions for reliable measurements. Subsequently, we inflated the robot and initiated vibration-assisted unburrowing. A typical experiment is depicted in Fig. 5. We tracked the marker location to determine the unburrowing depth, as shown in Fig. 6. A total of three unburrowing experiments were conducted, with an average unburrowing time of 2053 s for 300 mm (10 times the body height), corresponding to an average speed of 0.0049

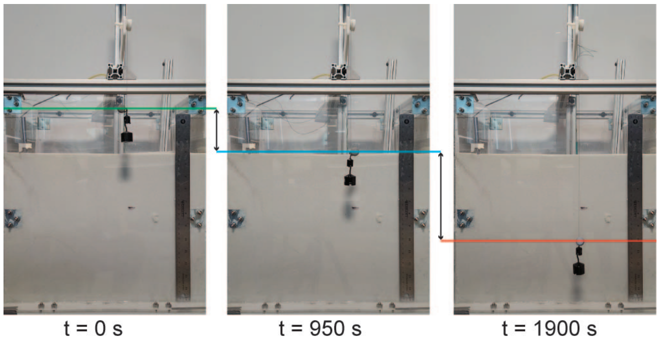

Fig. 5: Unburrowing experiments. We attached counter weight to the end of the tendon to compensate the resistance as well as keep the tendon straight to allow accurate measurement of the position of the robot. Since the robot was unburrowing upwards, the tracking marker was then moving towards the ground.

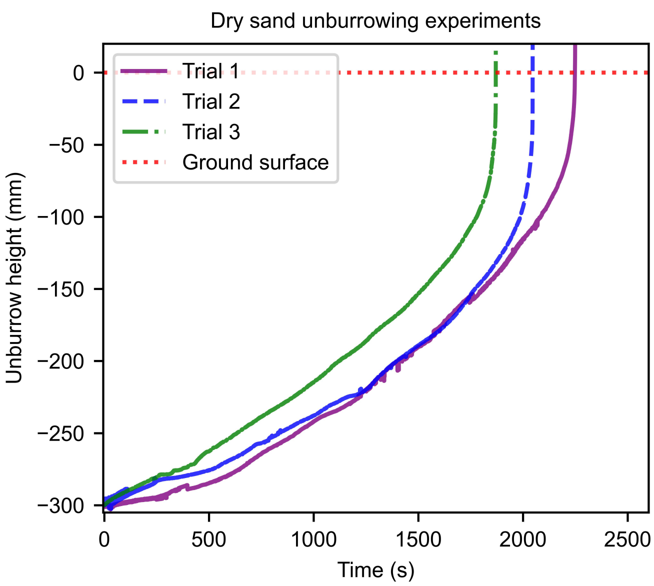

Fig. 6: Recorded height during unburrowing experiments measured using MoCap system. A total of three trials was performed, with the horizontal red line indicating the target depth. After 300 mm, the robot was out of the granular media, pulled by the tendon and counterweight, resulting in high moving speed.

body-heights-per-second. We observed deviation of the unburrowing performance, which we attribute to variation in the position of the robot at the start of the experiments. We suspect that the complex interaction between the soft pouch and the surrounding granular media generated arbitrary initial shape. Thus the initial conditions varied slightly resulting in differences in the rates of unburrowing.

C. Effect of vibration during unburrowing cycle

To further investigate the role of vibration in the unburrowing process, we conducted an experiment illustrated in Fig. 7. Initially, we placed an inflated robot with the counterweight attached in the granular media, but without activating the vibration motor. Despite the robot's density being lower than that of the surrounding media due to inflation, it remained stationary, as shown by the solid blue line in the green regions of Fig. 7. This highlights that volume change alone is insufficient for unburrowing.

At the 600-second mark, we activated the vibration motor. The robot immediately began to rise (red areas in Fig. 7), demonstrating the role of vibration-induced local fluidization in facilitating upward movement. After 600 seconds of unburrowing, we deactivated the vibration motor, and the robot again became stationary. This process was repeated, and the tracked height is shown for a total of 3000 seconds. We did not analyze the effect of vibration in the digging cycle, as without vibration and local fluidization, the robot is unable to penetrate the granular media and burrowing ceases.

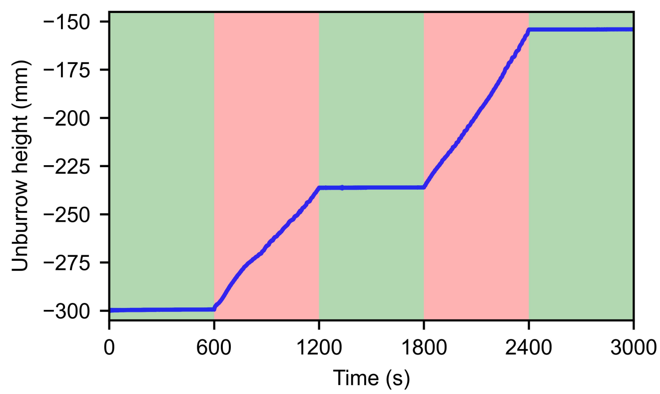

Fig. 7: Unburrowing height change with and without vibration (red vs. green). We started the robot at the bottom of the sand tank with the pouch inflated, indicated as the green area. The unburrowing height of the robot is indicated by the blue line. In the red region, both inflating and vibration were applied.

D. Anchoring and force measurement

We measured the anchoring force, described by the removal force of the robotics anchors when buried inside the granular media by recording the maximum force required for pulling out. Similar to the tether-induced force measurement in Sec. III-B, we first started the fluidization to minimize the intrusion resistance and place the robot at the bottom. We then used a force gauge[4] to pull the robot until a peak tension was recorded and the robot start moving.

We measured the anchoring force in four configurations: 1) unactuated robot, 2) deflated robot with vibration, 3) inflated robot without vibration and 4) inflated robot with vibration, corresponding to each state in the digging and unburrowing state (Fig. 8). In the deflated state, the robot was able to provide an anchoring force of up to 23.4 N while with vibration, the force reduced to 6.7 N. The anchoring force increased significantly to 35.0 N with the pouches inflated. In this case we attribute the increase to the high friction between the TPU soft pouches to granular media as well as increased contact area and compression. With the vibration and local fluidization while inflated, the drag reduced again to 32.3 N.

[4]Mark-10 Series 3

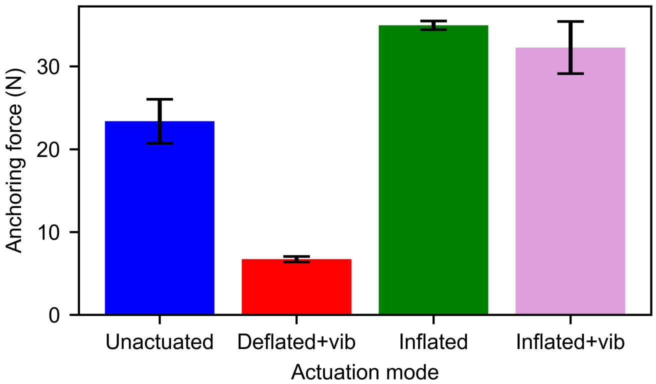

Fig. 8: Average anchoring force with standard deviation in different mode

IV. Conclusion and Future Work

In this paper, we presented a self-burrowing/unburrowing robot capable of traversing more than 10 times its body height in granular media using local fluidization and density tuning. We detailed the design inspiration, mechanism design, robotic realization, and experimental setup. We measured key performance metrics, including digging and unburrowing distances, the impact of TPU pouches, and the effect of vibration. Our results demonstrate the robot's ability to burrow and unburrow over 300 mm vertically by utilizing local fluidization and density tuning, requiring only a single volume change to switch between digging and unburrowing.

We observed that the soft TPU pouches significantly impacted digging speed due to friction, which potentially affected the unburrowing process as well. Consequently, a primary focus for future work could be reducing this friction. This includes optimizing the geometry of the pouch, exploring alternative materials with lower drag, and implementing a volume adjustment mechanism with shape optimized for reduced drag in granular media. Currently, we use glass beads of average diameters with air blowing for initialization to simulate loosely packed sand with a volume fraction of approximately 0.58, as commonly observed in nature [24]. Wider material selection is also crucial for locomotion in vario us granular media as well as increasing locomotion versatility, such as wet underwater sand, fine sand, and irregular sand, which is one of the major thrust of the future works.

Although the current robot design was tethered, requiring cables for power and air supply, we believe it has realistic potential for untethered operation. This is because the power consumption of the vibration motor is low (3.4 W). A lithium battery, such as a 3.7V CR123A battery with a typical capacity of 1.5Ah, could power the robot for approximately 97.94 minutes. This duration is sufficient for a complete digging/unburrowing cycle.

Furthermore, in the current design, air was utilized only for a single volume change, and an external pneumatic supply is currently employed. Future work could explore alternative air supply methods, including chemical reactions (e.g., combustion) [25], [26], phase-change materials (e.g., low boiling point fluids) [27], [28], or contained air sources such as CO_2 canisters [29], potentially enabling untethered operation.

Additional future work includes investigating the scalability of this design, determining the maximum achievable locomotion height, and assessing payload capacity at each scale. It would be interesting to analyze the effects of vibration power, fin dimensions, and equivalent density on digging and unburrowing performance. Such analyses would be crucial for selecting appropriate battery sizes for untethered operation. Following the evaluation of scalability, payload, and locomotion limits, a modular version of this anchoring soft robot with connectors will enable the creation of a digging robot swarm for increased system-level payload capacity.

Acknowledgment

This material is based upon work supported by the Office of Naval Research (ONR) under grant numbers N00014-23-1-2358 and N00014-23-1-2169. Any opinions, findings, and conclusions or recommendations expressed in this material are those of the author(s) and do not necessarily reflect the views of the ONR.

References

[1] H. Wei, Y. Zhang, T. Zhang, Y. Guan, K. Xu, X. Ding, and Y. Pang, "Review on Bioinspired Planetary Regolith-Burrowing Robots," *Space Science Reviews*, vol. 217, Nov. 2021.

[2] A. Hosoi and D. I. Goldman, "Beneath Our Feet: Strategies for Locomotion in Granular Media," *Annual Review of Fluid Mechanics*, vol. 47, no. 1, pp. 431–453, Jan. 2015.

[3] C. Le, O. D. Yirmibesoglu, S. Even, T. Buckner, Y. Ozkan-Aydin, and R. Kramer-Bottiglio, "Grand challenges for burrowing soft robots," vol. 12, publisher: Frontiers. [Online]. Available: https://www.frontiersin.org/journals/robotics-and-ai/articles/10.3389/frobt.2025.1525186/abstract

[4] E. Lauga, "Life around the scallop theorem," *Soft Matter*, vol. 7, no. 7, pp. 3060–3065, 2011.

[5] S. Huang and J. Tao, "Locomotion in Granular Media: A Geomechanical Perspective on Symmetry Breaking," vol. 2022, Mar. 2022, p. Q03.003.

[6] D. Li, S. Huang, Y. Tang, H. Marvi, J. Tao, and D. M. Aukes, "Compliant Fins for Locomotion in Granular Media," *IEEE Robotics and Automation Letters*, vol. 6, no. 3, pp. 5984–5991, Jul. 2021.

[7] S. Chopra, D. Vasile, S. Jadhav, M. T. Tolley, and N. Gravish, "Toward Robotic Sensing and Swimming in Granular Environments using Underactuated Appendages," *Advanced Intelligent Systems*, vol. 5, no. 8, p. 2200404, Aug. 2023.

[8] J. J. Tao, S. Huang, and Y. Tang, "SBOR: a minimalistic soft self-burrowing-out robot inspired by razor clams," *Bioinspiration & Biomimetics*, vol. 15, no. 5, p. 055003, Jul. 2020.

[9] H. Bagheri, D. Stockwell, B. Bethke, N. K. Okwae, D. Aukes, J. Tao, and H. Marvi, "A bio-inspired helically driven self-burrowing robot," *Acta Geotechnica*, vol. 19, no. 3, pp. 1435–1448, Mar. 2024.

[10] D. Luo, A. Maheshwari, A. Danielescu, J. Li, Y. Yang, Y. Tao, L. Sun, D. K. Patel, G. Wang, S. Yang, T. Zhang, and L. Yao, "Autonomous self-burying seed carriers for aerial seeding," *Nature*, vol. 614, no. 7948, pp. 463–470, Feb. 2023.

[11] P. Philippe and M. Badiane, "Localized fluidization in a granular medium," *Physical Review E*, vol. 87, 2013.

[12] w. A G, "Razor clam to RoboClam: burrowing drag reduction mechanisms and their robotic adaptation," *Bioinspiration & Biomimetics*.

[13] N. D. Naclerio, A. Karsai, M. Murray-Cooper, Y. Ozkan-Aydin, E. Aydin, D. I. Goldman, and E. W. Hawkes, "Controlling subterranean forces enables a fast, steerable, burrowing soft robot," *Science Robotics*, vol. 6, no. 55, p. eabe2922, Jun. 2021.

[14] N. D. Naclerio, C. M. Hubicki, Y. O. Aydin, D. I. Goldman, and E. W. Hawkes, "Soft Robotic Burrowing Device with Tip-Extension and Granular Fluidization," in *2018 IEEE/RSJ International Conference on Intelligent Robots and Systems (IROS)*, Oct. 2018, pp. 5918–5923.
[15] L. D. B. Passini, F. Schnaid, M. M. Rocha, and S. V. Möller, "Mechanism of model pile installation by water jet fluidization in sand," *Ocean Engineering*, vol. 170, pp. 160–170, Dec. 2018.
[16] K. Hashemnia and S. Pourandi, "Study the effect of vibration frequency and amplitude on the quality of fluidization of a vibrated granular flow using discrete element method," *Powder Technology*, vol. 327, pp. 335–345, Mar. 2018.
[17] K. Helal, T. Biben, and J. Hansen, "Local fluctuations in a fluidized granular medium," *Physica A: Statistical Mechanics and its Applications*, vol. 240, no. 1, pp. 361–373, Jun. 1997.
[18] S. B. Savage, "Streaming motions in a bed of vibrationally fluidized dry granular material," *Journal of Fluid Mechanics*, vol. 194, no. -1, p. 457, Sep. 1988.
[19] D. Goldman, F. L. Hammond III, and T. Wang, "Robust self-propulsion in sand using simply controlled vibrating cubes," *Frontiers in Robotics and AI*, vol. 11, Aug. 2024.
[20] B. Darbois Texier, A. Ibarra, and F. Melo, "Low-resistive vibratory penetration in granular media," *PLOS ONE*, vol. 12, no. 4, p. e0175412, Apr. 2017.
[21] W. Kang, Y. Feng, C. Liu, and R. Blumenfeld, "Archimedes' law explains penetration of solids into granular media," *Nature Communications*, vol. 9, no. 1, p. 1101, Mar. 2018.
[22] T. Shinbrot, "The brazil nut effect — in reverse," *Nature*, vol. 429, no. 6990, pp. 352–353, May 2004.
[23] N. Gravish, P. B. Umbanhowar, and D. I. Goldman, "Force and Flow Transition in Plowed Granular Media," *Physical Review Letters*, vol. 105, no. 12, p. 128301, Sep. 2010. [Online]. Available: https://link.aps.org/doi/10.1103/PhysRevLett.105.128301
[24] W. W. Dickinson and J. D. Ward, "Low depositional porosity in eolian sands and sandstones, namib desert," vol. 64, no. 2, pp. 226–232. [Online]. Available: https://doi.org/10.1306/D4267D66-2B26-11D7-8648000102C1865D
[25] C. A. Aubin, R. H. Heisser, O. Peretz, J. Timko, J. Lo, E. F. Helbling, S. Sobhani, A. D. Gat, and R. F. Shepherd, "Powerful, soft combustion actuators for insect-scale robots," *Science*, vol. 381, no. 6663, pp. 1212–1217, Sep. 2023.
[26] N. W. Bartlett, M. T. Tolley, J. T. B. Overvelde, J. C. Weaver, B. Mosadegh, K. Bertoldi, G. M. Whitesides, and R. J. Wood, "A 3D-printed, functionally graded soft robot powered by combustion," *Science*, vol. 349, no. 6244, pp. 161–165, Jul. 2015.
[27] S. M. Mirvakili, D. Sim, I. W. Hunter, and R. Langer, "Actuation of untethered pneumatic artificial muscles and soft robots using magnetically induced liquid-to-gas phase transitions," *Science Robotics*, vol. 5, no. 41, p. eaaz4239, Apr. 2020.
[28] S. Hirai, T. Nagatomo, T. Hiraki, H. Ishizuka, Y. Kawahara, and N. Miki, "Micro Elastic Pouch Motors: Elastically Deformable and Miniaturized Soft Actuators Using Liquid-to-Gas Phase Change," *IEEE Robotics and Automation Letters*, vol. 6, no. 3, pp. 5373–5380, Jul. 2021.
[29] Y. Zhai, A. De Boer, J. Yan, B. Shih, M. Faber, J. Speros, R. Gupta, and M. T. Tolley, "Desktop fabrication of monolithic soft robotic devices with embedded fluidic control circuits," *Science Robotics*, vol. 8, no. 79, p. eadg3792, Jun. 2023.